PERGAMON

International Journal of Impact Engineering 25 (2001) 641–660

INTERNATIONAL JOURNAL OF IMPACT ENGINEERING

www.elsevier.com/locate/ijimpeng

Normal impact of ogive nosed projectiles on thin plates

N.K. Gupta[a,*], R. Ansari[b], S.K. Gupta[a]

[a]*Department of Applied Mechanics, Indian Institute of Technology Delhi, Hauz Khas, New Delhi 110 016, India*
[b]*Department of Mechanical Engineering, Aligarh Muslim University, Aligarh 202 002, India*

Received 1 November 2000; received in revised form 16 February 2001

Abstract

Single plates of aluminium of various thicknesses were subjected to normal impact by ogive nosed projectiles at velocities normally greater than their ballistic limit. The observed values of the residual velocity and ballistic limit are presented and influence thereon of various parameters is discussed. Based on the mechanism of deformation observed and the data of residual and incident velocities, analytical and empirical relations have respectively been developed for the determination of both residual velocity and ballistic limit. These relations are seen to match the experiments well.

1. Introduction

The study of the impact of projectiles on thin plates has long been of interest, and several studies on the subject are available in literature. Comprehensive surveys on the subject have been published by Backman and Goldsmith [1]; Corbett et al. [2] and Goldsmith [3] which discuss various features of the phenomenon involved.

Most of the experimental impact studies on thin plates in sub-ordnance velocity range were carried out for d/h_0 ratio up to 10, in which generally plate of thicknesses (h_0) greater than 1.25 mm and projectile of diameters (d) up to 12.5 mm have been employed [4–10]. The studies of thin plates particularly impacted by ogive nosed projectiles in the higher range of d/h_0 ratio are not many.

The 12.5 mm diameter spherical or cylindro-conical projectiles were impacted by Calder and Goldsmith [4] at a velocity range of 25 to 300 m/s on 1.25 mm thick plate. They proposed a simplified model for central deflection of rigid-plastic linear work hardening material. They found that the simplifications they made for modelling of perforation phenomena, introduced incorrectness

* Corresponding author. Tel.: +91-11-659-1178; fax: +91-11-658-1119.
E-mail address: nkgupta@am.iitd.ernet.in (N.K. Gupta).

0734-743X/01/$ - see front matter
PII: S0734-743X(01)00003-3

Nomenclature

a	a constant depend upon the profile of the perforated plate
b	radius of the crater
D	depth of the crater
d	diameter of the projectile
E_{ab}	energy of the projectile absorbed by the plate
E_p	perforation energy
h_0	original thickness of the plate
k, n	constants depend upon the ballistic limit of the plate and impact velocity versus residual velocity curve
l	shank length of the projectile
l_n	nose length of the projectile
l_{cr}	length of the crack
m	mass of the projectile
r_p	radius of the projectile
s	span of the plate in between the supports
v_i	impact velocity of the projectile
v_r	residual velocity of the projectile
v_d	velocity drop of the projectile
v_{bl}	ballistic limit of the plate
w	deflection of the plate
w_c	deflection of the plate at the centre
Y	yield strength of the plate
σ_θ	circumferential stress
σ_r	radial stress
σ_u	ultimate tensile strength of the plate
ρ	density of the plate
v	Poisson's ratio

of results at low velocity impact, whereas, the results matched the experimental data at higher impact velocities.

Corran et al. [5] investigated the effect of projectile mass, nose shape and hardness on penetration of steel and aluminium alloy plates. Blunt and cylindro-conical projectiles of 12.5 mm diameter, were impacted on plates of 1.3 to 5.9 mm thickness in the velocity range of 50 to 250 m/s. The mass of the projectile was varied from 15 to 100 g. They observed that ballistic limit of the plate changes with change of projectile mass and nose shape.

Levy and Goldsmith [6] used instrumented projectiles having piezoelectric quartz disc inside the projectile body. Interchangeable heads of 6.35 and 12.7 mm diameters and three nose shapes viz. blunt, spherical and conical, were fitted onto the same instrumented projectile body. A detailed experimental study was made in the velocity range of 20 to 300 m/s, and on 1.27 and 3.175 mm thick aluminium plates and 1.2 mm thick mild steel plates. Impact load, permanent deflection and strain were measured with the help of instrumented projectile, optical profile projector and strain gauges,

respectively. Most of the observations were made just below and above the ballistic limit. The measured peak force and plate deflection of aluminium plate below the ballistic limit shows a good correlation with the values predicted by the model [7] but in the case of mild steel plates, the results show discrepancy.

Petalling is the dominant phenomenon in thin aluminium plates when struck by ogive-nosed or cylindro-conical projectiles at sub-ordnance velocities. Landkof and Goldsmith [8] carried out a theoretical and experimental investigation of petalling of thin metallic plates impacted by cylindro-conical projectiles. A model considering initial crack propagation, plastic hinge motion up to the root of the crack, and petal bending due to hinge rotation is presented. An experimental programme was carried out for verification of the model wherein 12.7 mm diameter cylindro-conical projectiles were impacted on 3.175 mm thick aluminium plates both with and without hole at their centre. Good correlation was found between the experimental and theoretical residual velocities except near ballistic limit.

Goldsmith and Finnegan [11] carried out an experimental programme of normal impact of cylindro-conical and blunt cylindrical projectiles of 12.7 mm diameter, on aluminium and steel plates at the velocity range of 20 to 1025 m/s. Projectiles of hard steel and soft aluminium were used in the study. Velocity drop during perforation was measured and metallurgical examination of the target damage was carried out on selected plates.

Virostek et al. [12] employed instrumented projectiles, similar to those used by Levy and Goldsmith [6], for recording force histories of normal impact of conical and hemispherical nosed projectiles on aluminium plates. The tests were carried out at impact velocities between 45 to 170 m/s. The effects of initial velocity and nose shape on the peak force have been studied. Simple models have also been developed to predict the peak force.

Liu and Stronge [13] presented three rigid plastic models, based on different assumptions for yield, for deformation of circular plate impacted by blunt projectiles. Bending and stretching of the plate and shearing of a plug at the centre of the plate is taken care of in the modelling. Computed results, based on these models, are compared with some experimental results available in literature.

In addition to the analytical studies, empirical relations for predicting the plate response have also been developed by researchers. Two fairly simple formulae which are being used for mild steel were developed by Stanford Research Institute (SRI) and the Ballistic Research Laboratories (BRL). SRI formula provides an estimate of the mean perforation energy of the plate for a particular target projectile system. Neilson [14] performed a dimensional analysis of experimental results for long rod penetrator ($l/d \geqslant 13$) and modified the SRI formula. The modified formula can estimate the mean as well as minimum perforation energy of mild steel plates. He felt that data were not enough for short penetrators to establish proper correlation between model and experimental values. Experimental results were deduced from existing data base.

Wen and Jones [9] proposed a semi-empirical equation using dimensional analysis, for the perforation energy in the case of mild steel plates struck by blunt projectiles. Energy absorbed by global structural response, including the effect of bending and stretching; and energy absorbed in shearing out a plug equal to projectile diameter were taken care of in the formulation. The results from this equation compared well with the impact test results of mild steel plates at low impact velocity.

An experimental investigation of normal and oblique impact of a spinning armour piercing projectile of core diameter 6.2 mm, on aluminium, mild steel and RHA steel plates of 6 to 40 mm

thicknesses were carried out by Gupta and Madhu [10,15]. Residual velocity, velocity drop and crater dimensions were measured. Simple models based on the experimental results were proposed for residual velocity, velocity drop, ballistic limit and critical ricochet angle.

In the present study, an extensive experimental programme has been carried out for relatively larger diameter ogive nosed projectiles and thinner aluminium plates, for which d/h_0 ratio varies from 7.5 to 30, to study the mechanism of deformation in detail. Experiments were performed on both single and layered plates. In the present paper, we discuss the response of single plates whereas behaviour of layered plates is discussed in a future paper. A mathematical model considering the mechanics of deformation observed during the experiments is presented. A simple empirical relation based on the experimental results is also developed for quick and easy assessment of the ballistic limit and other related parameters of the perforation process. Quasi-static test were performed on similar aluminium plates for comparison with the impact tests.

2. Experiments

The present study is concerned with the response of thin plates to the normal impact of a projectile. The plates employed were cut out of commercial purity aluminium ($\sim 99\%$) sheets of thicknesses 0.5, 0.74, 1.0, 1.5 and 2.0 mm. Circular targets of 255 mm total diameter with 205 mm diameter free span were made from these plates and used in as received condition. The projectile were essentially ogive nosed hardened steel with 2.0 caliber radius head and 10 and 15 mm diameter. Their Rockwell hardness were recorded as R_c 47–52. The length to diameter ratio (l/d) of 10 mm diameter projectile was varied from 1 to 4. The d/h_0 ratio in our experiments was varied from 7.5 to 30. Dimension of the projectile and strength of the target materials were measured and recorded in Tables 1 and 2. A pneumatic gun, shown in Fig. 1, of fixed barrel was used for firing the projectiles at velocities generally higher than the ballistic limit of the target.

Projectile carriers of teflon were used for accommodating projectiles of different sizes in the same barrel. The barrel had a stopper at its exit end for holding the carrier just before projectile leaves the barrel. Three infrared emitters and same number of photo diodes were fixed at known distances at the exit of the barrel to measure the impact velocity of the projectile. Residual velocities were measured with the help of two sets of aluminium foil screens of thickness 8 μm, placed behind the target plate. Data were recorded by electronic counter timer and digital storage oscilloscope (Gould 1604). The profiles of the deformed specimens were measured from the distal sides of the plates with the help of a dial gauge set-up.

Table 1
Dimension and mass of projectiles

Sl. no.	Diameter (mm)	l/d ratio	Total length (mm)	Mass (g)
1	10.0	1	23.24	10.35
2	10.0	2	33.30	16.7
3	10.0	3	43.32	23.0
4	10.0	4	53.24	28.8
5	15.0	2	49.6	55.0

Table 2
Tensile strength of the aluminium plates of different thicknesses

Sl. no.	Plate thickness (mm)	0.2% offset yield strength (MPa)	Ultimate tensile strength (MPa)
1	0.5	120	125
2	0.74	130	134
3	1.0	124	130
4	1.5	115	120
5	2.0	120	126

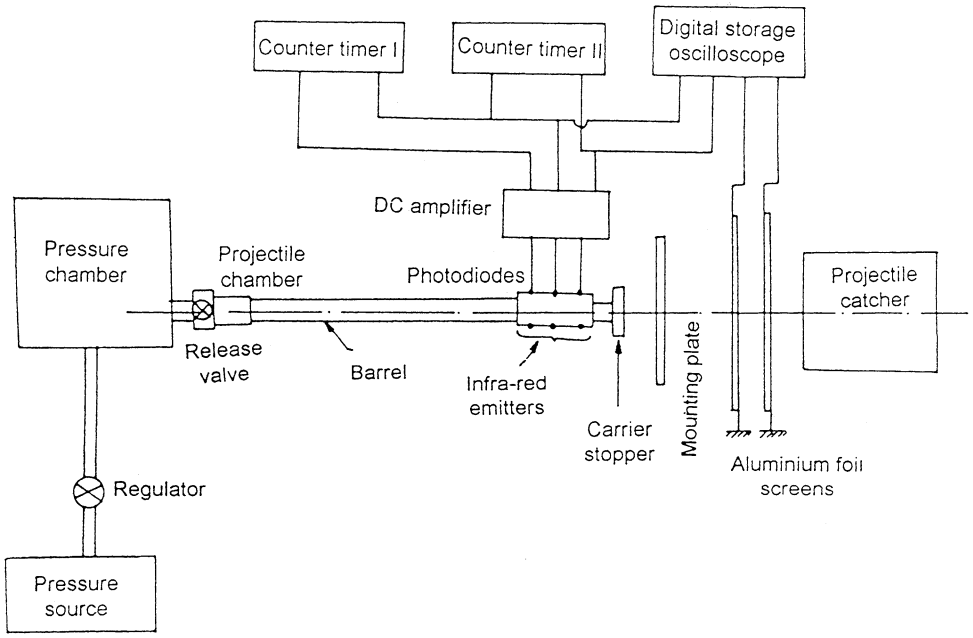

Fig. 1. Schematic diagram of the experimental set-up.

Quasi-static tests at a cross-head speed of 1 mm/min were performed on aluminium plates under the condition similar to that of impact tests on MTS 810 machine. Details of the test procedure are described in Ref. [16]. The energy absorbed by the plates were calculated from the load deformation curve.

3. Experimental results

3.1. Effect of plate thickness

Typical measured values of the residual velocity of 15 mm diameter projectile are plotted against impact velocity in Fig. 2 for aluminium plates of all thicknesses employed. The residual velocity

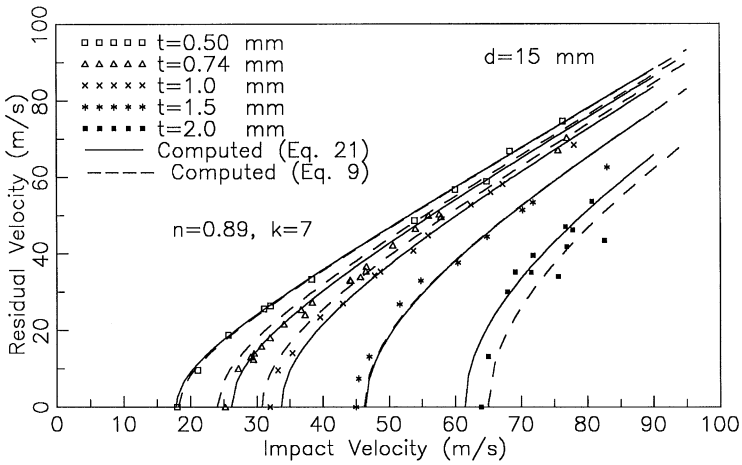

Fig. 2. Experimental results of residual velocities versus impact velocities for aluminium plates of different thicknesses along with curves obtained from Eqs. (9) and (21).

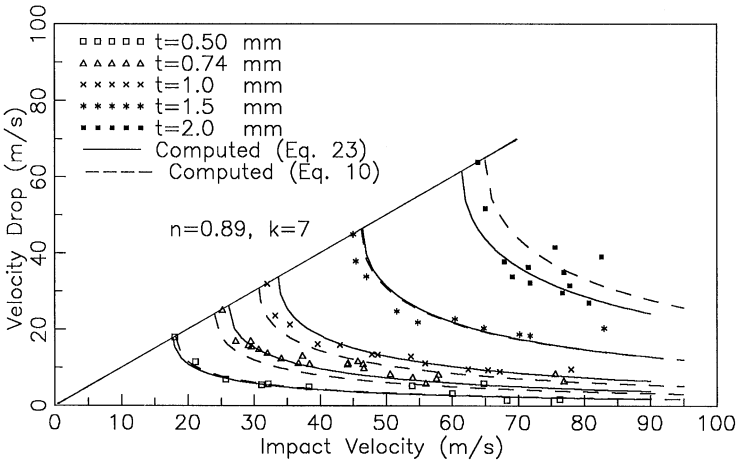

Fig. 3. Comparison of experimental velocity drop for aluminium plates of different thicknesses with results obtained from Eqs. (10) and (23).

increases with increase of impact velocity for each plate. This increase is rapid near the ballistic limit and later the curve tends to become parallel to the asymptote of unit slope. The variation of velocity drop with the impact velocity is shown in Fig. 3. The velocity drop decreases steeply near the ballistic limit and afterward it tends to be constant. The effect of impact energy on the energy of the projectile absorbed by the plate during perforation are shown in Fig. 4. The absorbed energy is almost constant at different impact energy/velocities of the projectile for a particular plate thickness, in the velocity range employed. The absorbed energy increases with increase of plate thickness.

The ballistic limit and critical perforation energy of single aluminium plates are plotted against plate thickness in Fig. 5(a) and against mass of projectile in Fig. 5(b). The ballistic limit increases

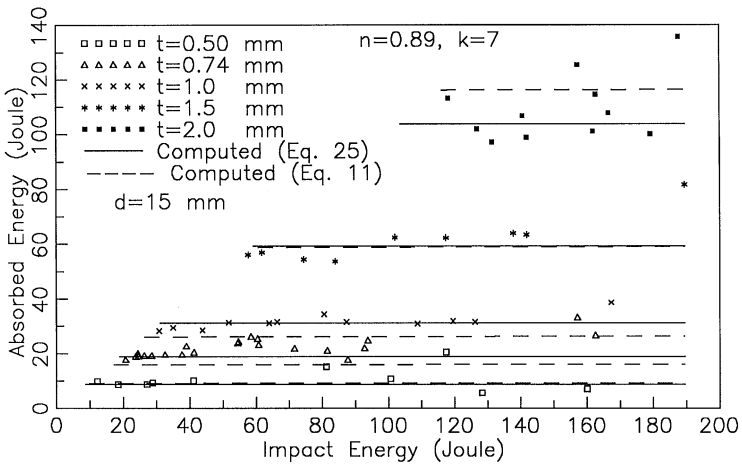

Fig. 4. Comparison of experimental absorbed energy for aluminium plates of different thicknesses with results obtained from Eqs. (11) and (25).

with increase of plate thickness and for a constant plate thickness it decreases with increase of projectile mass. The perforation energy increases with increase of plate thickness and it shows no change with increase in mass of the projectile for the same plate thickness.

The final shapes of the deformed plates were measured with the help of a dial gauge set-up. It is seen that overall bending of the plate (dishing) and localised deformation near the point of impact, increases with increase of plate thickness for all thicknesses and all velocities above the ballistic limit. The dishing and bulging are also sensitive to the velocity of impact. It is seen from Fig. 6, that for same plate thickness the dishing varies with impact velocity and it reduces with increase in velocity of impact above ballistic limit. Typical profiles of the plates deformed in quasi-static tests and their comparison with the plates subjected to dynamic tests are shown in Fig. 6. This show that dishing increases with increase of plate thickness in quasi-static tests but it is less in comparison to their values in dynamic tests. It is known [4] that for impact velocities lower than ballistic limits, the deflection increases with increase in velocity of impact.

The energy absorbed by aluminium plates of different thicknesses in quasi-static and dynamic perforation are given in Table 3. It shows that the absorbed energy increases with increase of plate thickness but the energy absorbed by the plate in a quasi-static test is less than the energy absorbed in a dynamic test. The absorbed energy in a quasi-static test is about 60 to 70% of the energy absorbed in a dynamic test.

3.2. Effect of l/d ratio or mass of the projectile

Figs. 7 and 5(b) show that the effect of projectile aspect ratio (l/d) and its mass, respectively, on critical perforation energy and ballistic limit of the plate is not significant. But the ballistic limit decreases sharply in the beginning and then slowly afterwards, with increasing l/d ratio or mass of the projectile. It is seen that the effect of l/d ratio on the profile of the deformed plate is insignificant.

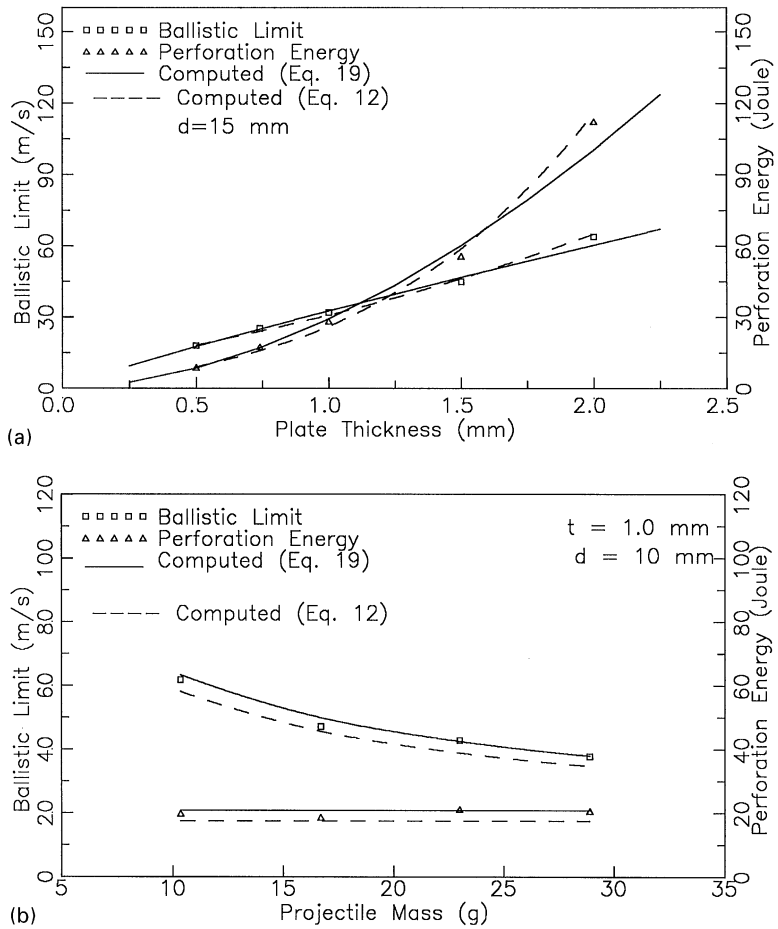

Fig. 5. (a) Comparison of experimental ballistic limit and critical perforation energy for aluminium plates of different thicknesses with results obtained from Eqs. (12) and (19). (b) Comparison of experimental ballistic limit and critical perforation energy for aluminium plates impacted with projectiles of different mass with results obtained from Eqs. (12) and (19).

3.3. *Effect of projectile diameter*

Fig. 8 shows the responses of aluminium plates of two different thicknesses when impacted by projectiles of 10 and 15 mm diameters and of l/d ratio equal to 2. It is found that, for a particular plate thickness, there is a change in residual velocity, velocity drop and energy absorbed by the plate when impacted by projectiles of different diameters. The trends of the plots of these parameters are similar for both projectiles of same l/d ratio. Fig. 8 shows that residual velocity increases with increase of impact velocity and it also increases with increase of projectile diameter for a particular plate thickness at a given impact velocity. The velocity drop is seen to decrease with increase of projectile diameter for a particular plate thickness at a given impact velocity and nature of this decrease is similar to that shown in Fig. 3. The absorbed energy is almost constant with

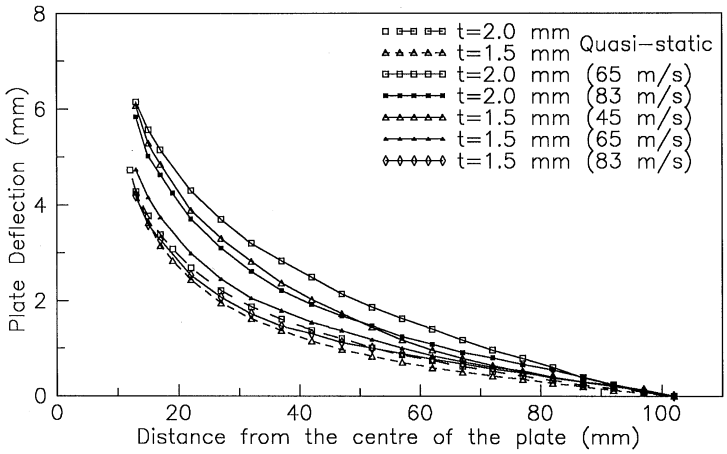

Fig. 6. Comparison of plate profiles of single aluminium plates, perforated in quasi-static and dynamic tests, of 1.5 and 2.0 mm thicknesses.

Table 3
Response of single aluminium plates in quasi-static test

Sl. no.	Quasi-static test (Strain rate-1 mm/min)					Dynamic energy 'E_p' (J)
	Specimen no.	Plate thickness (mm)	Peak load (N)	Total energy (J)	Total energy % of 'E_p'	
1	St A11	2.0	2550	75.6	67.3	112.3
2	St M12	1.5	1650	39.2	78.6	55.7
3	St D12	1.0	856	19.7	69.9	28.2
4	St G12	0.74	550	11.0	62.9	17.5
5	St J13	0.5	280	4.9	55.1	8.9

increase of impact velocities however, it increases with increase of projectile diameter for a particular plate thickness.

4. Mechanism of deformation of thin aluminium plates

It is observed during experiment that in perforation of thin aluminium plates by ogive nosed projectile, its tip first makes an indent in the plate followed by the yielding of the plate around the tip of the projectile and dishing in rest of the plate, as shown in Figs. 9(a) and (b). The plate deforms in the shape of projectile nose at its centre and with further deformation, the tip of the projectile comes out and cracks initiate at the tip of the crater which propagate and form petals with movement of the projectile. The yielding of the plate in the contact region is verified by measuring the thicknesses of the petals at different points from the tip of the petal with the help of a pointed tip screw gauge and are given in Table 4.

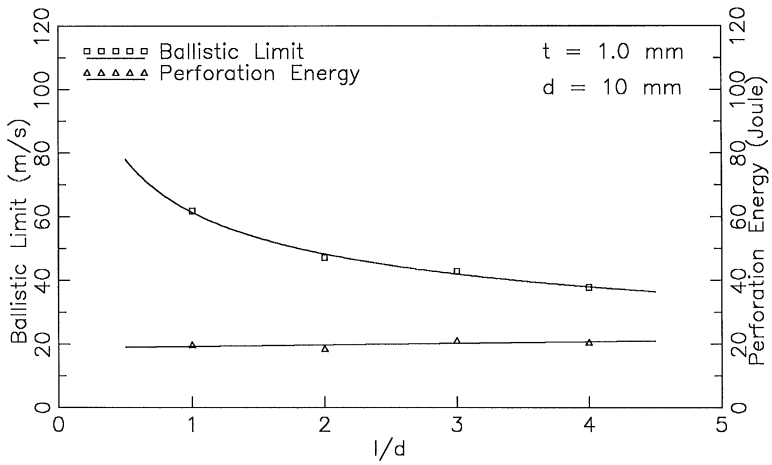

Fig. 7. Variation of critical perforation energy of single aluminium plates, impacted by 10 mm diameter projectiles, with l/d ratio of the projectile.

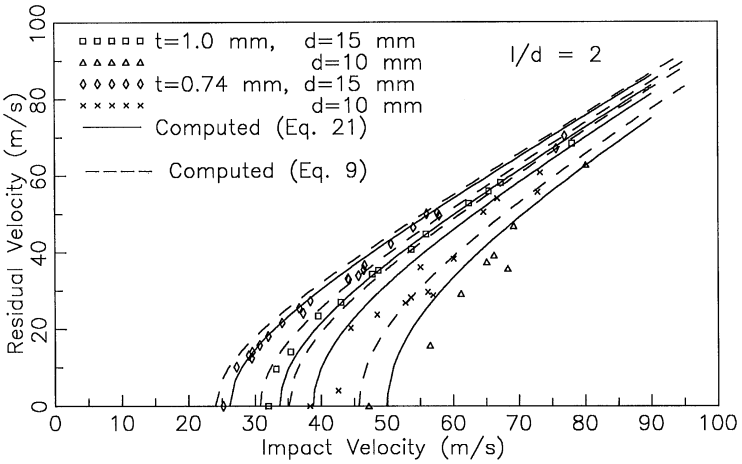

Fig. 8. Comparison of experimental residual velocities for aluminium plates impacted with projectiles of 10 and 15 mm diameters with results obtained from Eqs. (9) and (21).

The measured values show the variation of the thickness from tip to the root of the petal in plates of all thicknesses. With further movement of the projectile the petals start rotating outward by the action of rolling hinges in plates of 0.5 and 0.74 mm thicknesses (for which d/h_0 is 30 and 20, respectively) and to some extent in 1.0 mm thick plate (d/h_0 is 15). The hinges seems to be rolling due to the frictional force present between the surface of plate and projectile. This small frictional force seems to be enough for the rolling of the hinges in plates where d/h_0 is more than 15. This process continues until the shank reaches at the root of the petals; the petal tip rotates beyond 90° (see Fig. 10). In plates of 1.5 and 2.0 mm thickness, the cracks initiated at the tip of the crater

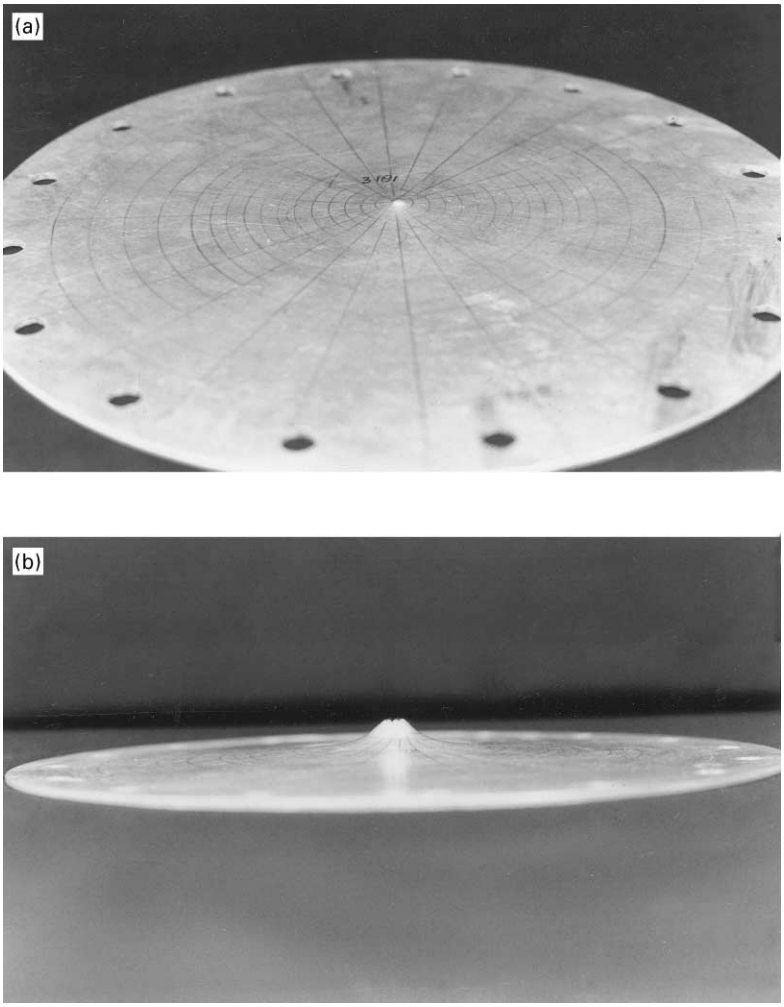

Fig. 9. (a) Aluminium plate showing indent at the centre of the plate. (b) Aluminium plate showing yielding around the centre and dishing in rest of the plate.

Table 4
Thickness of the petal at different points and average crack length

Sl. no.	Distance from tip of the petal (mm)	Thickness of the petal (mm) of plates of different thicknesses			
		2.0 mm	1.5 mm	1.0 mm	0.74 mm
1	0	0.46	0.45	0.48	0.47
2	2	1.18	1.04	0.86	0.65
3	4	1.46	1.24	0.95	0.69
4	6	1.80	1.31	0.95	—
Average crack length (mm)		7.5	8	9	9.5

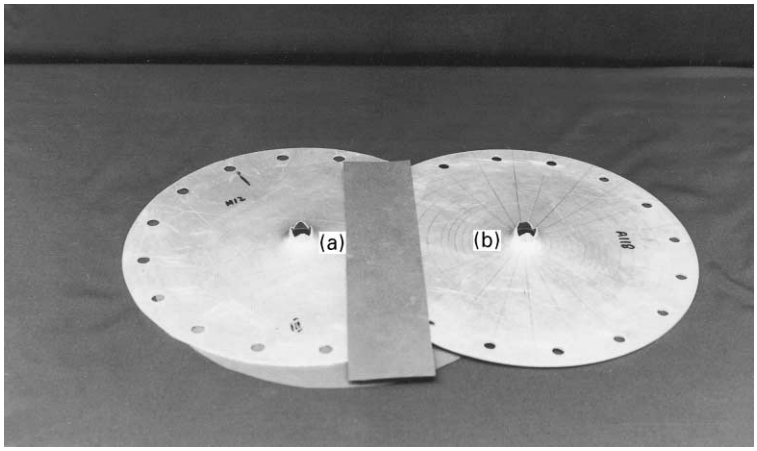

Fig. 10. Aluminium plates of 0.5 and 0.74 mm thicknesses showing rotation of petals above 90°.

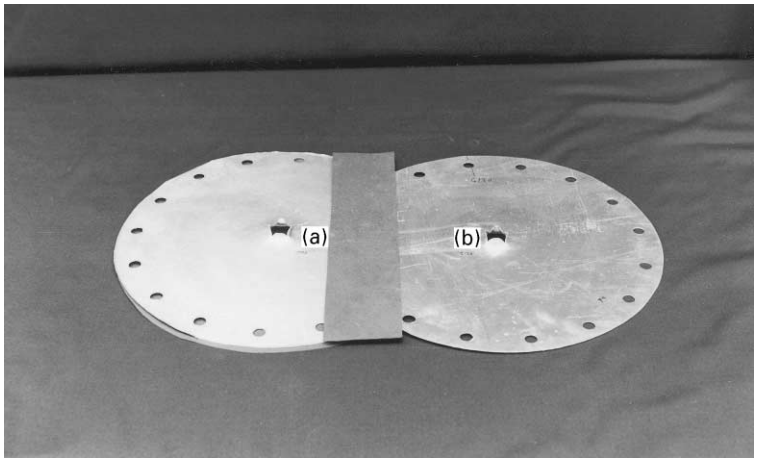

Fig. 11. Aluminium plates of 1.5 and 2.0 mm thicknesses showing rotation of petals about 90°.

propagates with the movement of the projectile and petals are formed. These petals bend along with the movement of projectile up to 90° from the surface of the plate. The cracks are arrested at this juncture and it is observed that the full circumference around the projectile nose start rolling till the shank reaches at the root of the crater. So there is no sign of rotation of the petal beyond 90° (see Fig. 11). The petal rotation up to 90° seems to be due to the action of bending of the petal by projectile nose in thicker plates. The petal rotation of a 1.0 mm thick plate lies in between the two described above, and the rotation of it is a little above 90°. The crack length or the edge length of the petals were also varied in plates of different thicknesses. It was maximum in plate of 0.5 mm thickness and minimum in 2.0 mm thick plate.

5. Analysis

The experimental observation shows that the primary mode of failures in a aluminium plate are yielding and petalling in the contact region along with dishing in rest part of the plate, when impacted by ogive nosed projectile. Thus, the total deformation of the plate may be divided into two types of deformation.

1. Deformation of the plate in the contact region of the plate and projectile.
2. Deformation of the plate in remaining part of the plate.

The first kind of deformation is the yielding and formation of petals in the distal side of the thin plates. Yielding seems to be a dominant phenomenon in this region because the energy absorbed in crack propagation and friction, which is responsible for the formation of petal, is small [8] and may be neglected. So, it is reasonable to assume this type of deformation as formation of a crater of diameter equal to the diameter of projectile at the centre of the plate (see Fig. 12) and the energy absorbed in it may be calculated from Thomson's model [17] with following assumptions:

1. Circumferential stress σ_θ is the only significant stress in the crater so that σ_{r}, σ_z may be assumed to be zero.
2. Plastic deformation takes place under stress $\sigma_\theta = Y$, Y is the yield stress.
3. Plastic deformation takes place without a change of volume.

Thus the work required in the formation of crater by ogive nosed projectile [2] is,

$$W_1 = \pi r_{\mathrm{p}}^2 h_0 \left[\frac{1}{2} Y + 0.62\rho \left(\frac{v_{\mathrm{i}} r_{\mathrm{p}}}{l_{\mathrm{n}}} \right)^2 \right]. \tag{1}$$

The second part of deformation of the plate when impacted by a projectile at low or medium velocity is the deformation of the plate in the region other than contact region. This is basically radial stretching (dishing) of the plate which absorbs major portion of the projectile energy in this velocity range.

The energy of the radial stretching due to the radial stress σ_{r} and radial strain ε_{r} (neglecting the circumferential stress) are evaluated as [4],

$$W_2 = \int_v \left(\int \sigma_{\mathrm{r}} \, \mathrm{d}\varepsilon_{\mathrm{r}} \right) \mathrm{d}V, \tag{2}$$

where

$$\varepsilon_{\mathrm{r}} = \left(\frac{\partial w}{\partial r} \right)^2. \tag{3}$$

The lower limit of the Eq. (2) is taken as the length of the crack, l_{cr}, and the upper limit is taken as infinity, since the contribution from the outer plate radius is small.

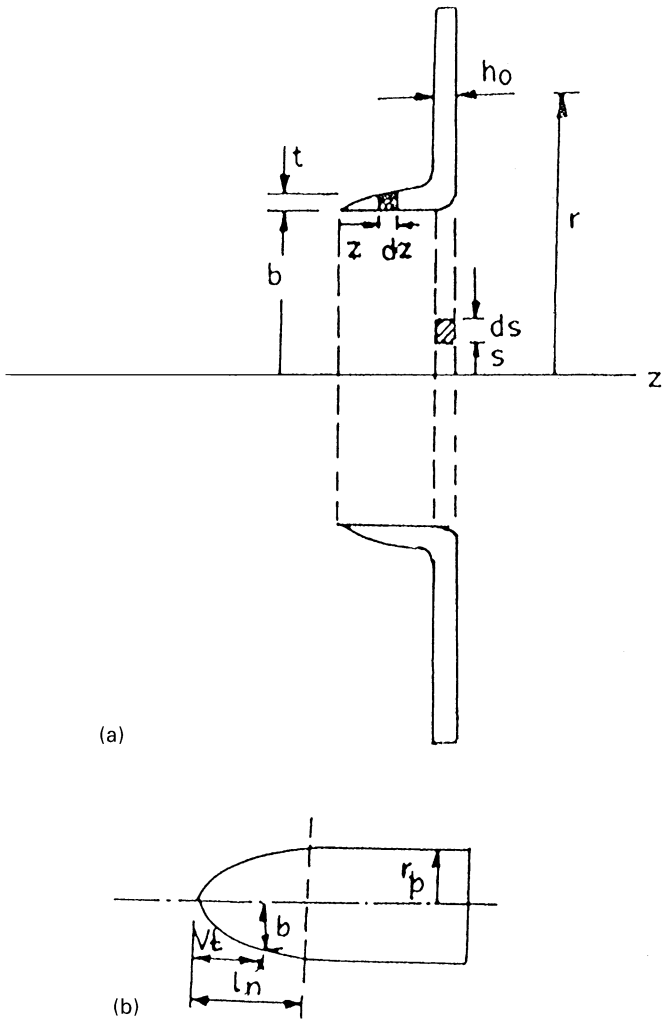

Fig. 12. (a) Crater of diameter equal to the diameter of the projectile [17]. (b) Geometry of the projectile [17].

The radial plate deflection w in the low or medium velocity range can be expressed (see [4]) as,

$$w = w_c e^{-ar}, \tag{4}$$

where w_c is the central deflection of the plate, a is a constant, which can be evaluated from the profile of the plate and r is the arbitrary radius of the plate.

Neglecting the work hardening and putting

$$\sigma_r = Y \tag{5}$$

the Eq. (2), after substituting Eqs. (3)–(5) into it, may be written as

$$W_2 = \frac{2\pi h_0 w_c^2}{(1 - v + v^2)^{1/2}}\left[\frac{e^{-2al_{cr}}}{8}(1 + 2al_{cr})Y\right]$$
$$= \frac{\pi h_0 w_c^2 Y e^{-2al_{cr}}(1 + 2al_{cr})}{4(1 - v + v^2)^{1/2}}, \tag{6}$$

where v is the Poisson's ratio.

Now the total work done in deformation of the plate, is

$$W = W_1 + W_2$$
$$W = \pi r_p^2 h_0\left[\frac{1}{2}Y + 0.62\rho\left(\frac{v_i r_p}{l_n}\right)^2\right] + \frac{\pi h_0 w_c^2 Y e^{-2al_{cr}}(1 + 2al_{cr})}{4(1 - v + v^2)^{1/2}}. \tag{7}$$

The equation of the energy balance, then may be written as

$$\frac{1}{2}mv_i^2 = \frac{1}{2}mv_r^2 + W. \tag{8}$$

So, the residual velocity of the projectile is

$$v_r = \sqrt{v_i^2 - \frac{2W}{m}}. \tag{9}$$

Using the Eq. (9), residual velocities of the projectiles for different combinations of plates and projectiles employed, were computed. These are shown as the dash lines in Figs. 2 and 8. These show good agreement with the experimental results.

The velocity drop of the projectile may be written as

$$v_d = v_i - v_r$$
$$= v_i - \sqrt{v_i^2 - \frac{2W}{m}}. \tag{10}$$

The dash lines in Fig. 3 show the computed values of the velocity drop of the projectiles for different combinations of plates and projectiles employed, using Eq. (10). These match well with experimental values.

The energy absorbed by a plate, E_{ab} may be written as

$$E_{ab} = W. \tag{11}$$

The dash lines in Fig. 4 show the computed values of the absorbed energy for different combinations of plates and projectiles employed, using Eq. (11) and they match well with experimental values.

The two components of energy viz. the energy required for the formation of crater in the contact region (W_1) and the energy of radial stretching in rest of the plate (W_2) are separately plotted against plate thickness in Fig. 13. It shows that W_1 decreases with increase of plate thickness

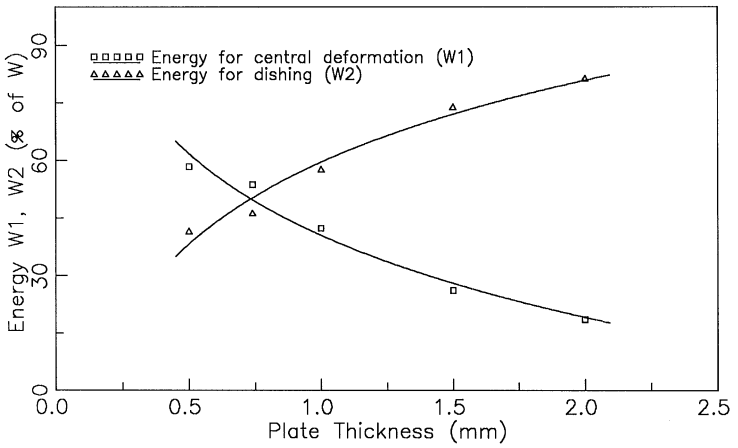

Fig. 13. Variation of components of total energy absorbed with plates of different thickness.

whereas W_2 increases with increase of plate thickness. In other words, major portion of the projectile energy goes in radial stretching of plates of thicknesses greater than 0.74 mm.

The ballistic limit of the plate can be written as

$$v_{\mathrm{bl}} = \sqrt{\frac{2W}{m}}. \tag{12}$$

The computed values of the ballistic limit for different combination of plate and projectile are shown by dash lines in Fig. 5(a) and (b), and they match well with experimental values.

6. Empirical relation

The plots of residual velocity and impact velocity for aluminium plates of different thicknesses are shown in Fig. 2. The curves show a definite pattern of the data for all five thicknesses of the plates. Initially, there is a steep rise in residual velocity with increase in impact velocity near the ballistic limit. With further increase in impact velocity the curve between residual velocity and impact velocity tends to be almost parallel to the asymptote of unit slope passing through the origin.

This data can be fitted in the form of an equation of a hyperbola, whose major axis is parallel to x-axis as shown in Fig. 14, and whose equation is

$$\frac{(x - x_0)^2}{a_1^2} - \frac{(y - y_0)^2}{b_1^2} = 1, \tag{13}$$

where a_1 and b_1 are half the lengths of the major and minor axes, respectively.

The slope of the asymptotes $G'H$ and GH' is $\pm b_1/a_1$. The slope of the asymptote is equal to unity which implies that

$$\frac{b_1}{a_1} = 1 \quad \text{or} \quad b_1 = a_1. \tag{14}$$

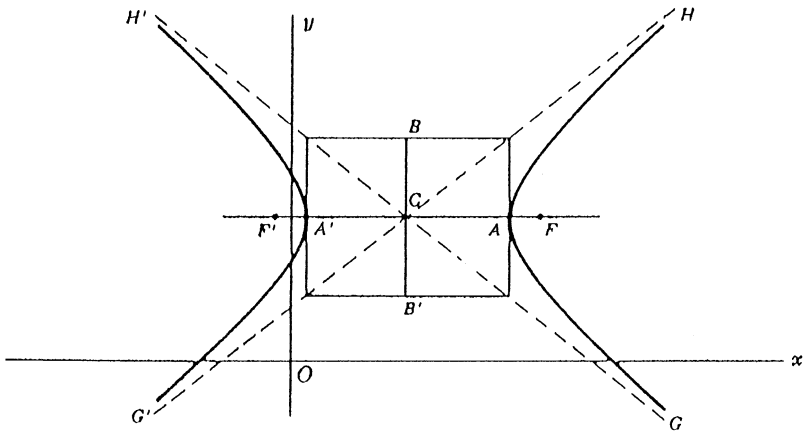

Fig. 14. A hyperbola with its major axis parallel to x-axis.

Eq. (13) becomes

$$x^2 - y^2 = a_1^2. \tag{15}$$

a_1 is found to be equal to the ballistic limit of the plate, v_{bl} (see Fig. 2).

Putting the parameters of x and y axes in Eq. (15), we get

$$v_i^2 - v_r^2 = a_1^2 \quad \text{or} \quad v_i^2 - v_r^2 = v_{bl}^2. \tag{16}$$

It is also seen from the experiment that the ballistic limit of the plate is related to the thickness of the plate (h_0), diameter (d) and mass (m) of the projectile, and the material properties of the plate.

Fig. 5(a) shows that the ballistic limit of the plate has a power relationship with its thickness. So, v_{bl} may be written as

$$v_{bl} \propto h_0^n. \tag{17}$$

Fig. 5(b) shows that the critical perforation energy of the plate i.e. the perforation energy of the plate at ballistic limit is constant with varying mass of the projectile for a given plate thickness.

$$E_{cr} = \frac{1}{2} m v_{bl}^2 = \text{constant}.$$

So, v_{bl} may be written as

$$v_{bl} \propto \sqrt{\frac{1}{m}}. \tag{18}$$

Fig. 8 shows that the ballistic limit of the plate increases with increase of the diameter of the projectile for same plate thickness. Considering these, along with the strength of the material of the

plate, the ballistic limit may be presented as

$$v_{bl} = \sqrt{\frac{kdY}{m}} h_0^n, \tag{19}$$

where, k and n are constants and Y is the yield strength of the material of the plate.

The values of k and n found from the experiments, for different combinations of projectiles and aluminium plates employed, are $k = 7$ and $n = 0.89$, when all the parameters of Eq. (19) are in SI units. The solid lines in Fig. 5a and b are the plots obtained from this equation and these match the experimental results well.

Now the Eq. (16) can be written as

$$v_i^2 - v_r^2 = \frac{kdY}{m} h_0^{2n}, \tag{20}$$

$$v_r = \sqrt{v_i^2 - \frac{kdY}{m} h_0^{2n}}. \tag{21}$$

The solid lines in Figs. 2 and 8 are the plots obtained from Eq. (21) and these match the experimental results well.

The velocity drop, v_d may be written as

$$v_d = v_i - v_r. \tag{22}$$

From Eqs. (21) and (22), we get

$$v_d = v_i - \sqrt{v_i^2 - \frac{kdY}{m} h_0^{2n}}. \tag{23}$$

The solid lines in Fig. 3 show the results obtained from Eq. (23) and these match the experimental results well.

The variation of absorbed energy by the plate is plotted against the impact energy in Fig. 4. The energy absorbed by the plate, during perforation, may be evaluated by the difference of the kinetic energy of the projectile before and after impact. This may be written as

$$\begin{aligned} E_{ab} &= \frac{1}{2} m v_i^2 - \frac{1}{2} m v_r^2 \\ &= \frac{1}{2} m (v_i^2 - v_r^2). \end{aligned} \tag{24}$$

From Eqs. (21) and (24) we get,

$$E_{ab} = \frac{1}{2} kdY h_0^{2n}. \tag{25}$$

The curves computed from Eq. (25) are shown as solid lines in Fig. 4 and they match well with the experimental values.

6.1. Comparison of experimental data with some empirical relations

There are some empirical relations being fairly used for the prediction of the perforation energy of plates impacted by projectiles. Some of these equations are [14].

(a) SRI equation:

$$\frac{E_p}{\sigma_u d^3} = \frac{42.7}{10.3}\left(\frac{h_0}{d}\right)^2 + \frac{1}{10.3}\left(\frac{s}{d}\right)\left(\frac{h_0}{d}\right), \tag{26}$$

(b) BRL equation:

$$\frac{E_p}{\sigma_u d^3} = \frac{1.4\times 10^9}{\sigma_u}\left(\frac{h_0}{d}\right)^{1.5}, \tag{27}$$

(c) Equation proposed by Wen and Jones [9]:

$$\frac{E_p}{\sigma_u d^3} = \left(\frac{2\sigma_y}{\sigma_u}\right)\left[\frac{\pi}{4}\left(\frac{h_0}{d}\right)^2 + \left(\frac{s}{d}\right)^{0.21}\left(\frac{h_0}{d}\right)^{1.47}\right], \tag{28}$$

(d) Equation proposed by Neilson [14]:

$$\frac{E_p}{\sigma_u d^3} = 1.4\left(\frac{s}{d}\right)^{0.6}\left(\frac{h_0}{d}\right)^{1.7}, \tag{29}$$

where E_p is the perforation energy, σ_u is the tensile strength and 's' is the unsupported span of the plate.

Experimental data of the present study of five different thicknesses of aluminium plates and two diameters of ogive nosed projectiles are compared with these empirical equations and are shown in Fig. 15. It is interesting to note that good correlation exists between the experimental data and the

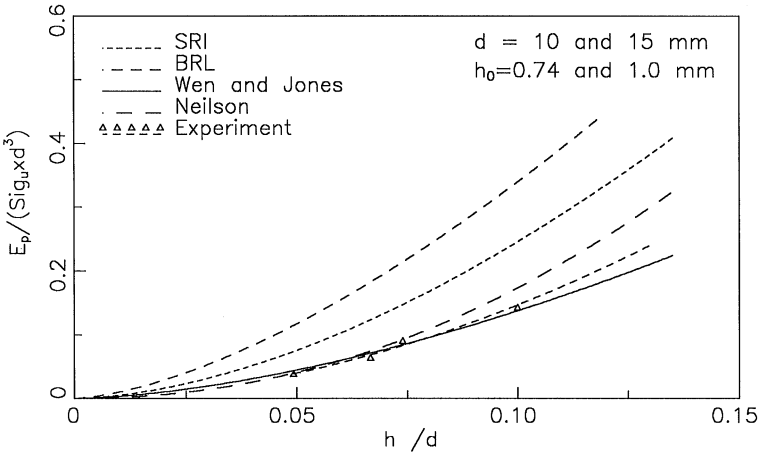

Fig. 15. Comparison of experimental results for plates impacted with projectiles of 10 and 15 mm diameter with existing empirical relations.

values predicted by Wen and Jones equation, except for 2.0 mm thick plate, even though these equations were developed for prediction of perforation energy of mild steel plates impacted by blunt projectiles.

7. Conclusions

The present study is carried out to generate experimental data of perforation of thin plates when impacted by ogive nosed projectiles. Based on the mechanism of deformation observed, analytical expression applicable to these mechanism are presented. Simple empirical relations are developed to determine the residual velocity and the ballistic limit. Results from both analytical and empirical expression are seen to match the experimental results very well.

References

[1] Backman ME, Goldsmith W. The mechanics of penetration of projectiles into targets. Int J Engng Sci 1978;16:1–99.
[2] Corbett GG, Reid SR, Johnson W. Impact loading of plates and shells by free-flying projectiles: a review. Int J Impact Engng 1996;18:141–230.
[3] Goldsmith W. Non-ideal projectile impact on targets. Int J Impact Engng 1999;22:95–395.
[4] Calder CA, Goldsmith W. Plastic deformation and perforation of thin plates resulting from projectile impact. Int J Solids Struct 1971;7:863–81.
[5] Corran RSJ, Shadbolt PJ, Ruiz C. Impact loading on plates—an experimental investigation. Int J Impact Engng 1983;1:3–22.
[6] Levy N, Goldsmith W. Normal impact and perforation of thin plates by hemispherically tipped projectiles—II, Experimental results. Int J Impact Engng 1984;2:299–324.
[7] Levy N, Goldsmith W. Normal impact and perforation of thin plates by hemispherically tipped projectiles—I, Analytical considerations. Int J Impact Engng 1984;2:209–29.
[8] Landkof B, Goldsmith W. Petalling of thin, metallic plates during penetration by cylindro-conical projectiles. Int J Solids Struct 1985;21:245–66.
[9] Wen H.-M. Jones N. Semi-empirical equations for the perforation of plates struck by a mass. In: Bulson PS, Editor. Structures under shock and impact II. Southampton, Boston: Computational Mechanics Publications, 1992. p. 369–80.
[10] Gupta NK, Madhu V. Normal and oblique impact of a kinetic energy projectile on mild steel plates. Int J Impact Engng 1992;12:333–43.
[11] Goldsmith W, Finnegan SA. Normal and oblique impact of cylindro-conical and cylindrical projectiles on metallic plates. Int J Impact Engng 1986;4:83–105.
[12] Virostek SP, Dual J, Goldsmith W. Direct force measurement in normal and oblique impact of plates by projectiles. Int J Impact Engng 1987;6:247–69.
[13] Liu D, Stronge WJ. Perforation of rigid-plastic plate by blunt missile. Int J Impact Engng 1995;16:739–58.
[14] Neilson AJ. Empirical equations for the perforation of mild steel plates. Int J Impact Engng 1985;3:137–42.
[15] Gupta NK, Madhu V. An experimental study of normal and oblique impact of hard-core projectile on single and layered plates. Int J Impact Engng 1997;19:395–414.
[16] Ansari R. Normal and oblique impact of projectiles on single and layered thin plates. Ph.D. thesis, IIT Delhi, 1998.
[17] Thomson WT. An approximate theory of armor penetration. J App Mech 1955;26:80–2.